Ultrafast two-dimensional NMR spectroscopy using constant acquisition gradients

Yoav Shrot and Lucio Frydman[a)]
Department of Chemical Physics, Weizmann Institute of Science, 76100 Rehovot, Israel

(Received 11 September 2006; accepted 17 October 2006; published online 28 November 2006)

Multidimensional NMR spectroscopy plays an important role in the characterization of molecular structure and dynamics. A new methodology for acquiring this kind of spectra has been recently demonstrated, endowed with the potential to compress arbitrary multidimensional NMR acquisitions into a single scan. This "ultrafast" nD acquisition protocol is based on a spatiotemporal encoding of the indirect-domain spin evolution, followed by a repetitive decoding and reencoding of the information thus stored employing a train of alternating-sign gradients. Such train of switching gradients extending throughout the course of the data acquisition may pose extreme demands on a magnetic resonance system, particularly when dealing with nonshielded gradients, strong eddy currents, or rapidly relaxing spin systems. Limits to the *in vivo* applicability of such fast-switching scheme may also arise due to gradient-induced perineural stimulation. The present study describes a new approach to ultrafast nD NMR that reduces the number of gradient switchings during the acquisition period to zero, leading in essence to a constant-gradient acquisition scheme. This approach operates on the basis of a novel spatiotemporal encoding including discrete, temporally overlapping, frequency-shifted pulses. Principles and examples of this new approach are given; sensitivity limitations and signal-enhancing prospects of such constant-gradient acquisitions are also discussed and exemplified. © *2006 American Institute of Physics*.
[DOI: 10.1063/1.2393233]

I. INTRODUCTION

Multidimensional nuclear magnetic resonance (nD NMR) plays a central role in numerous areas of contemporary research. It serves as a basis for numerous *in vitro* analyses of molecular structure and dynamics, and acts as a basic tool for clinical diagnosis within the context of *in vivo* NMR spectroscopy.[1–3] The information content of multidimensional NMR exceeds that of its one-dimensional (1D) counterparts thanks to the presence of new cross-peak correlations, while its resolving power is greatly augmented by the presence of multiple dimensions on which to spread the various resonances. The conventional implementation of nD NMR involves coupling onto a direct-domain acquisition, a series of parametrically incremented delays whereby individual experiments probe every point in the remaining $(n-1)$ time dimensions to be explored.[1–5] Standard resolution and bandwidth criteria define the data sampling needs along every axis of the time domain, implying that the overall duration required to complete such nD acquisition is not always dictated by sensitivity considerations but rather by the need to fulfill Nyquist criteria along all of the indirect-domain dimensions. Recently we have proposed a general methodology capable of collapsing arbitrarily high multidimensional NMR acquisitions, into a single-scan experiment.[6–8] Such "ultrafast" scheme replaces the series of time-incremented scans making up an nD acquisition with a spatiotemporal manipulation, whereby different spatial elements throughout the sample volume are charged with encoding the various indirect-domain evolution times. This partitioning of the sample enables one to encode the full indirect-domain information being sought within a single scan, thus potentially reducing the duration of this kind of experiments by several orders of magnitudes. New practical applications that could be opened up by this approach include the realization multidimensional NMR experiments on prepolarized spins and on continuously flowing samples, as well as the utilization of 2D NMR to follow dynamic biophysical and metabolic processes.[9–12]

A number of variants have been described in the literature in order to implement these single-scan two-dimensional (2D) NMR acquisitions;[7,13–17] all of them based on a common scheme whereby the indirect-domain interactions to be measured are initially encoded in space with the aid of frequency-shifted pulses and magnetic field gradients. Then, following a mixing stage, this spectral information is read out multiple times during a data acquisition period happening in conjunction with the oscillation of a magnetic field gradient. The various ultrafast 2D protocols hitherto proposed differ in the ways by which the indirect-domain evolution of the spins is to be spatially encoded. An initial spatial encoding proposal was based on the application of a discrete, frequency-incremented train of excitation radio frequency (rf) pulses, implemented in synchrony with a rapidly switching $\pm G_e$ gradient whose oscillation echoed away the dephasing effects introduced by the gradient itself [Fig. 1(A)].[6,7] Although general in its applicability this discrete spatial encoding mode was found demanding in terms of its

[a)]Electronic mail: lucio.frydman@weizmann.ac.il

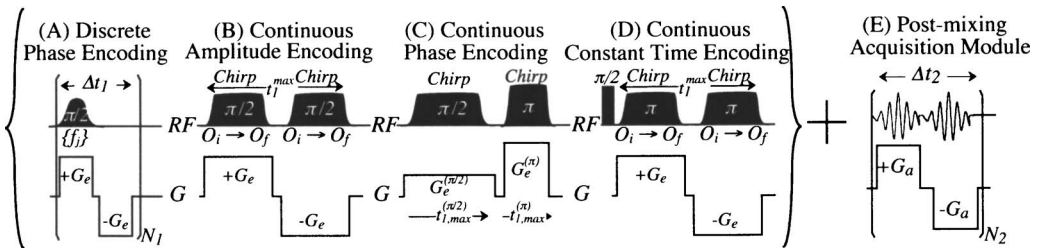

FIG. 1. Summary of the main strategies described so far for acquiring spatially encoded 2D NMR spectra within a single scan. (A) Discrete encoding protocol composed of a train of N_1 rf pulses applied at frequencies $\{f_i\}_{i=1,N_1}$ separated by constant increments ΔO and acting in combination with an oscillatory gradient $\pm G_e$. [(B)–(D)] Continuous frequency-swept variants whereby the discrete selective pulses in (A) are replaced by either $\pi/2$ excitation/storage or by π inversion pulses, and the spatial encoding is implemented in the presence of only two different gradients. (E) Following the mixing period data are digitized while subjecting spins to a periodic, sign-alternating acquisition gradient $\pm G_a$ oscillating numerous N_2 times; this demand for an oscillating acquisition gradient throughout the digitization period has been common to all the encoding strategies hitherto proposed.

hardware requirements, as its rapid and accurate switchings of the excitation gradient challenge NMR hardware capabilities. This discrete encoding mode was also found endowed with "ghosting" features along the indirect domain,[7] whose elimination was often deemed convenient.[18] In consequence, a number of additional approaches based on the combined application of a single bipolar gradient and of continuous frequency-swept encodings of the interactions were subsequently proposed [Figs. 1(A)–1(D)].[13–16] The reliance of all these variants on a single switch of the encoding gradient alleviates considerably the demands imposed by the original discrete scheme on the hardware, while the continuous character of these encoding modes eliminates the appearance of repetitive indirect-domain "ghost peaks" during the course of the acquisition. Constant- as well as real-time, and amplitude- as well as phase-modulated versions of these continuous spatial encoding modalities were demonstrated based on such frequency-chirped spatial-encoding procedures.

And yet, these various continuous encoding alternatives provide only a partial solution to the fast-gradient switching problem. Indeed all of these variations, such as their initial discrete counterpart, still rely on the application of an oscillatory acquisition gradient train $\pm G_a$ for the sake of repetitively reading out $2N_2$ indirect-domain spectra as a function of the acquisition time t_2. The fact that these acquisition gradients can be shaped to smoothly oscillating functions certainly makes their application less demanding than those associated with the original square-wave excitation gradient train.[9] Yet complications may still arise if eddy currents become non-negligible, if spin relaxation times are short compared to the gradient switching times, as well as in *in vivo* cases where bandwidths may demand large gradient slew rates reaching the limit of perineural stimulation.[19,20] It is to account for this kind of problems that the present research work proposes a new ultrafast 2D acquisition modality that reduces *all* gradient oscillations, both over the course of the excitation as well as during the acquisition periods, to a minimum. In particular, a new encoding modality that enables the use of a fixed, constant-valued gradient throughout the entire course of the data digitization process is hereby discussed. We proceed in the following sections to describe the basic physics of this new proposal, illustrate its experimental performance, and introduce a series of sensitivity-enhancement refinements to this scheme.

II. THEORETICAL DESCRIPTION OF CONSTANT-GRADIENT ULTRAFAST 2D NMR ACQUISITIONS

A. Physical principles of the experiment

Like for all the ultrafast 2D NMR variants that have been hitherto demonstrated, the encoding of the evolution frequencies underlying our new constant-gradient acquisition scheme will still proceed by associating different indirect-domain evolution times t_1 with corresponding spatial elements. In other words, assuming the typical case of a z gradient assisting the encoding, we shall still demand that the indirect time-domain variable fulfills $t_1=C(z-z_0)$, with $C=dt_1/dz$ a spatiotemporal coefficient under our control. Given a chemical shift and/or J-coupling Ω_1 to be measured over t_1, this will then endow transverse coherences with incremented evolution phases along the sample's z axis: $\phi_e(z)=C(z-z_0)\Omega_1$. Considered over the full sample the resulting winding of coherences will lead to no observable signal; yet if the detection is carried out while applying a gradient G_a of z geometry during the acquisition, an additional phase term $\int_0^{t_2}\gamma_a G_a(t')dt'z=kz$ will be imparted leading to a constructive interference of all volume elements and to an observable echo at $k=-C\Omega_1$. Ultrafast 2D NMR relies on this decoding feature to read out the indirect-domain frequency spectrum. Moreover, given such k-based readout of the Ω_1 interactions, the simplest way to obtain the full $I(k/\nu_1,\nu_2)$ 2D data set being sought within a single continuous acquisition consists of periodically reversing this spectral decoding process by oscillating the sign of the G_a gradient. The evolution of the indirect-domain k/ν_1 spectra can then be repeatedly monitored for each point along the t_2 axis, and a 1D Fourier transform (FT) of the resulting interferograms along t_2 will thereby yield the desired 2D spectrum. All single-scan 2D NMR approaches presented thus far were based on such periodic sign alternations of the acquisition gradients, illustrated for completion in Fig. 1(E).

This oscillating-G_a solution, however, turns out not to be unique, and other means are also available to create a train of indirect k/ν_1 spectra as a function of t_2. In fact the ghost peaks mentioned earlier were an actual example of that: these were indirect-domain echoing phenomena that appeared repeatedly during the course of the signal acquisition, even though spins were being subject to the action of a *constant* acquisition gradient. These multiple echo peaks were

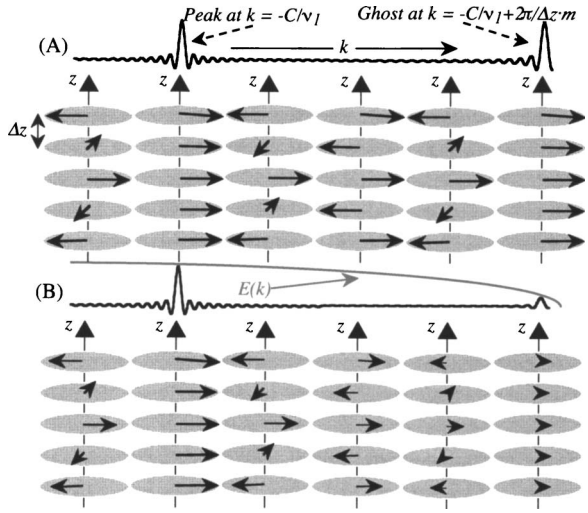

FIG. 2. (A) Idealized origin of the multiple ghost-peak echoes arising along the indirect dimension of discrete 2D ultrafast NMR experiments. The fact that in this scheme all spin packets are excited at constant offset differences ΔO implies that they are equally spaced, and consequently will come into constructive interference repetitively at time intervals given by $\gamma_e G_e/(\Delta O \gamma_a G_a)$ (or speaking in k-axis units, in multiples of $2\pi/\Delta z$). (B) Actual pattern expected in the intensities of the main vs flanking ghost peaks, from the ultrafast NMR experiment introduced in (A). The illustrated differences in relative intensities result from intraslice rephasing/dephasing processes imparted by G_e and G_a (illustrated by a variation in the spin-packet intensities with time), and are summarized by the shown $E(k)$ enveloping function.

seen in the past implementations as an unnecessary complication worth suppressing.[18] By contrast, the goal of the present study is to show how such echoes can be exploited for the sake of completing both amplitude- and phase-modulated single-scan nD experiments, while avoiding the need for repetitive oscillations of the G_a acquisition gradient. Multiple indirect-domain "ghost" peaks arose upon applying a train of selective N_1 pulses at constant offset increments ΔO and time increments Δt_1, while under the action of a constant gradient G_e (Fig. 2). Such excitation mode created a set of discrete transverse spin packets positioned at constant spatial separations $\Delta z = \Delta O/\gamma_e G_e$, carrying the indirect-domain encoding in their discretely incremented evolution phases $\{\phi_e(z_n) = Cn\Delta z\Omega_1\}_{n=1,N_1}$. Upon being subject to the postmixing acquisition gradient G_a these isochromats accumulate an additional evolution phase $kz_n = k(n\Delta z + z_0)$, z_0 denoting the sample's arbitrary origin. In its simplest form, the signal arising from such experiment will then be given by

$$S(k) = A\sum_{n=1}^{N_1} \exp(iCn\Delta z\Omega_1)\exp(ikz_n)$$

$$= A\exp(ikz_0)\sum_{n=1}^{N_1} \exp(in(C\Omega_1 + k)\Delta z). \quad (1)$$

For a sufficiently large number of spin packets the summations will exhibit sharp destructive and constructive interference phenomena, and an echo mapping the indirect-domain frequency will thus form as desired at $k = -C\Omega_1$. Yet in addition to this observable signal, echoes will also arise whenever the condition

$$k = -C\Omega_1 + \frac{2\pi}{\Delta z}m, \quad m = \pm 1, \pm 2, \ldots \quad (2)$$

is fulfilled. It is from this multiple solution that the multiple echoes alluded to earlier—the ghost peaks—will originate. An illustration of this phenomenon is presented in Fig. 2(A) using a simplified "five-sliced" spin-packet profile as an example.

Both this cartoon as well as Eq. (2) predict the appearance of an infinite train of periodic echoes along t_2, arising while under the action of a constant gradient. As all these echoes correspond to multiple repeats of the indirect-domain spectrum yet appear at different acquisition times, they could in turn provide a possibility of acquiring the full 2D $S(k/\nu_1, t_2)$ interferogram being sought, without requiring the multiple G_a oscillations that complicate the single-scan 2D acquisition. In practice, however, both the equation and the figure entail a simplification: they assume that spin packets conform to an idealized discrete structure, which neglects the finite width of the slices and thereby the *intraslice* dephasing that G_a will cause during the course of the signal acquisition. The destructive interference that thus sets in within each spin packet results in a k-dependent modulation of their intensities and an overall decay of the ghosts' amplitudes, as schematically illustrated in Fig. 2(B). Within a linear approximation, such echo decay as a function of k can be described by an enveloping function $E(k)$ depending on a variety of parameters related to the rf pulse shapes $P(t)$ used to impose the discrete encoding,[7,21]

$$E(k) \propto P\left(\frac{\gamma_e G_e T_p/2 - k}{\gamma_e G_e}\right). \quad (3)$$

In the simple case of the excitation being triggered by identical, rectangular rf pulses of duration T_p,

$$P(t) = \begin{cases} 1, & 0 < t < T_p \\ 0, & o.w. \end{cases}$$

and the train of detectable echoes will exhibit a nonzero and uniform value only over a limited range of acquisition wave numbers. This range will be given by $\Delta k = \gamma_e G_e T_p$, which in combination with Eq. (2) predicts that the number of "ghost" echoes to be detected will be confined to

$$N_2 \approx \frac{\Delta k \Delta z}{2\pi} = \frac{(\gamma_e G_e T_p)(\Delta O/\gamma_e G_e)}{2\pi} = \frac{\Delta O T_p}{2\pi}, \quad (4)$$

where ΔO is the offset increment involved in the application of the selective pulse train.

The ultrafast 2D NMR spectroscopy experiments hitherto implemented using discrete excitation pulses relied on offset increments and pulse lengths that optimized the adjacency between neighboring voxels. That is, they had the rf's offset increments ΔO and pulse lengths T_p optimized in relation to one another so as to make $N_2 \approx 1$. By contrast, the constant-gradient protocol that we are hereby proposing aims at creating multiple echoes; each of these representing the progression of the individual k/v_1 interferograms along t_2. It follows from Eq. (4) that this can be done by extending the individual pulse widths T_p so as to make their duration ex-

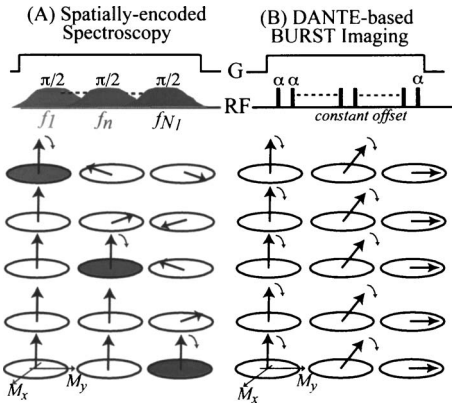

FIG. 3. Comparison between two discrete schemes proposed for the single-scan encoding of MR data based on the excitation of discrete, uniformly spaced, narrowband spin packets. (A) Ultrafast 2D spectroscopy scheme presented in this study and involving the application of an overlapping train of frequency selective $\pi/2$ pulses, spaced at constant frequency and time increments. Each pulse excites a specific volume element that begins to evolve immediately thereafter, providing a linear relation between the spin packet's position z and t_1. Notice that the narrowness of each pulse's bandwidth leads to a partial excitation of the sample. (B) Imaging scheme based on the application of a small-nutation DANTE pulse train, characterized by a single frequency offset and gradually affecting a set of equally spaced spin packets simultaneously.

ceed the $\Delta O T_p \approx 1$ condition. This in turn may lead to a temporal overlap between the individual rf pulses making up the overall spin excitation train, with each rf pulse in the train commencing before the irradiation of the previous components is complete [Fig. 3(A)]. Setting in such manner the offsets involved in the pulse train according to $T_p \gg (\Delta O)^{-1}$ will lead to narrow, well-separated voxels, and prevent from every one of the excited slices to become affected by the action of more than one of the sequential pulses. On the other hand reliance on such temporally overlapping train of frequency-incremented pulses also forces the use of a constant, nonoscillatory excitation gradient G_e throughout the course of the spatial encoding; as there no longer is then a possibility of reversing the effects of G_e in between the overlapping excitation pulses [as in Fig. 1(A)], the echoing of the G_e-derived effects will have to be addressed at a latter stage of the 2D sequence.

Before proceeding with a detailed description on how this idea can be fully implemented, it may be relevant to compare the similarities and differences that the resulting protocol will exhibit *vis-à-vis* another pulse sequence that also relies on the use of "thin" and well-separated slices: the DANTE-based BURST single-scan 2D magnetic resonance imaging (MRI) sequence.[22–24] As illustrated in Fig. 3(B) this sequence is also based on the excitation of discrete elements in the presence of a G_e gradient, and on the detection of multiple echoes generated by the action of a subsequent constant acquisition gradient G_a. The initial multiple-slice pattern, however, is in this case generated by the application of a DANTE sequence,[25] composed by a train of small-nutation rf pulses that excite simultaneously a series of well-separated, equidistant spatial elements. By contrast, the time- and frequency-shifted pulse train on which the new ultrafast proposal here introduced relies [Fig. 3(A)] carries out such excitation sequentially, giving an opportunity to encode the internal interactions affecting the spins during the indirect domain along the z spatial dimension. Still, as in the case of BURST, such choice of "thin" and well-separated excitation voxels will decrease the fraction of the overall magnetization that is excited, and thereby result in losses of the experiment's overall sensitivity. Dealing with this will require departing from the simple, rectangular-like amplitude modulation assumed so far for each $P(t)$ discrete excitation pulse, and replacing it with a more sophisticated phase-modulated wave form. This possibility will be analyzed and exemplified later on in this presentation; before this, we turn to an in-depth description on how to implement full ultrafast 2D NMR spectral acquisitions based on the encoding scheme in Fig. 3(A).

B. General description of constant-gradient ultrafast 2D NMR experiments

The use of a polychromatic rf train made up of N_1 selective, temporally shifted pulses is necessary but not sufficient to obtain the desired encoding of the indirect-domain Ω_1 interactions. Indeed, a pulse scheme like the one illustrated in Fig. 3(A) will excite over a series of incremented indirect-domain evolution times $\{t_1(n)=(N_1-n)\Delta t_1\}_{n=1,N_1}$ a series of spin isochromats precessing at rotating-frame offsets $\{f_n=[n-(N_1/2)]\Delta O\}_{n=1,N_1}$. Yet in spite of their differing frequencies, the isochromats excited by these pulses will fail to differentiate the internal Ω_1 frequencies we are attempting to measure from the external contribution of the G_e gradient acting upon them—both of which appear combined in the frequency's definition as $\{f_n=\Omega_1+\gamma_e G_e z_n\}_{n=1,N_1}$. Similar problems emerged in the development of continuous spatially encoding schemes,[13–16] and were dealt with by using subsequent spatially selective rf manipulations executed while under the effects of a different gradient strength G_e'. Also for the new discrete excitation scheme that is here discussed we propose to deal with this problem by employing either storages or inversions of the spin magnetizations under the action of a separate $G_e' \neq G_e$ gradient [Fig. 4(A)], which enables us to differentiate couplings and shifts from position-based frequencies.

To define the overall conditions that these manipulations will have to fulfill we begin by deriving the overall evolution phases imparted by these combined rf and gradient pulses, on arbitrary spins within the sample. To do so it becomes convenient to describe the fate of spins at any given z coordinate in terms of two parameters: an index n directly associated with the encoding frequencies f_n defining, in combination with an *a priori* unknown Ω_1 interaction, each of the discrete central-slice positions z_n, and an off-center displacement δz whose distribution will eventually define the nature of the enveloping function $E(k)$ characterizing the course of the t_2 acquisition. Following the various definitions given so far, these positions can be described as

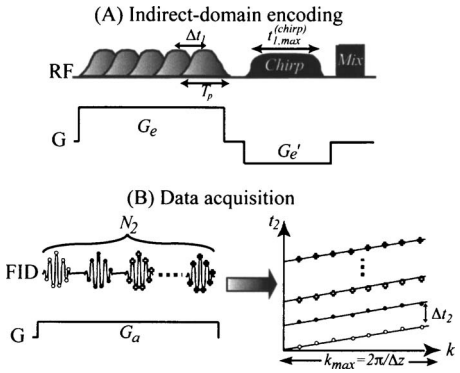

FIG. 4. Generic strategy for the single-scan acquisition of 2D NMR spectra using a constant acquisition gradient. (A) Discrete spatial encoding pattern achieved by a train of N_1 temporally overlapping selective pulses of duration T_p, separated by time and frequency offset increments of Δt_1 and ΔO. This discrete excitation is carried out while applying a constant gradient G_e, and is followed by either a storage or inversion of the spin coherences while in the presence of a second constant gradient G'_e. This last manipulation is performed using a continuously swept rf pulse as described in the text. (B) Following the mixing period, a series of N_2 echoes is generated by the action of a constant acquisition gradient G_a. These periodic indirect-domain echoes then arising in the FID are arranged into a 2D matrix representing the k/ν_1 and the t_2 evolutions as illustrated by the lower right-hand panel. FT of the N_2 echoes resulting along t_2 then provides the 2D $I(\nu_1,\nu_2)$ NMR spectrum being sought.

$$z(n,\delta z)=\frac{\Delta O}{\gamma_e G_e}(n-N_1/2)-\frac{\Omega_1}{\gamma_e G_e}+\delta z \tag{5a}$$

$$=qn+p+\delta z, \tag{5b}$$

with the spread $-(2\gamma_e G_e T_p)^{-1}\leqslant\delta z\leqslant(2\gamma_e G_e T_p)^{-1}$ inversely proportional to the duration T_p of the rf pulse exciting the nth spatial voxel. The phases $\varphi_{\rm exc}$ accumulated by spins at arbitrary positions can then be expressed as

$$\varphi_{\rm exc}(n,\delta z)=[\Omega_1+\gamma_e G_e z(n,\delta z)]t_1(n)+\phi_{\rm rf}(n)+\phi_{\delta z} \tag{6a}$$

$$=\left[\left(n-\frac{N_1}{2}\right)\Delta O+\gamma_e G_e\delta z\right]\times\left[(N_1-n)\Delta t_1+\frac{T_p}{2}\right]+\phi_{\rm rf}(n)+\phi_{\delta z}. \tag{6b}$$

Notice that besides the first term, representing overall phases precessed by each of the elements and assumed to begin accruing immediately following each spin-packet's excitation, Eq. (6) introduces two additional phase contributions: an overall shift $\phi_{\rm rf}(n)$ under our control and denoting the phase employed upon applying each of the selective rf pulses making up the excitation train, as well as an intraslice $\phi_{\delta z}$ dephasing term associated with $E(k)$ which, under the assumption that identical pulse shapes $P(t)$ were used to define all rf wave forms of the excitation train, we shall assume is independent of n. Further expansion of the product in Eq. (6b) leads to a polynomial that is quadratic in n (i.e., in position) and linear in δz; disregarding from now on irrelevant constant-phase terms one ends up with

$$\varphi_{\rm exc}(n,\delta z)=an^2+bn+cn\delta z+d\delta z+\phi_{\rm rf}(n)+\phi_{\delta z}, \tag{7a}$$

where

$$a=-\Delta O\Delta t_1,\quad b=\left(\frac{3N_1}{2}\Delta t_1+\frac{T_p}{2}\right)\Delta O,$$
$$c=-\gamma_e G_e\Delta t_1,\quad d=\left(N_1\Delta t_1+\frac{T_p}{2}\right)\gamma_e G_e. \tag{7b}$$

The quadratic n dependence in Eq. (7), arising from the product of incremented temporal and frequency elements, cannot be refocused by the linear field gradient to be applied during the acquisition and therefore has to be removed for the sake of observing the desired echoes. We shall do so by an appropriate choice of the $\phi_{\rm rf}(n)$ phases used to excite each of the discrete elements, as this constitutes one of the variables under our control. Also in need of removal is the $n\ \delta z$ term, which endows each of the voxels that is being excited with a nonuniform dephasing of its own, and thereby conspires against the acquisition of the constant train of echoes that we are trying to achieve. To account for this second effect—and to eventually leave solely the internal Ω_1 features that we wish to unravel encoded linearly as a function of n—we shall rely on a second stage of spatial-encoding manipulations; this time characterized by the use of a different gradient strength $G'_e\neq G_e$. As mentioned, this second manipulation could involve either a frequency-chirped storage of the excited magnetizations along a longitudinal state, or a spatially dependent refocusing of transverse magnetizations. As either one of these additional manipulations must address each and every voxel that was excited by the initial pulse train, it is convenient to have them based on continuous $\pi/2$- or π-based frequency-swept schemes such as those introduced in Figs. 1(B)–1(D), rather than on a discrete set of storage or inversion pulses. As discussed elsewhere the application of either one of these $\pi/2$ or π chirped pulses will also lead to quadratic phase-encoding profiles,[13–16]

$$\varphi_{\rm sweep}(z)=\alpha z^2+\beta z+\gamma, \tag{8a}$$

where

$$\alpha;\beta;\gamma=\begin{cases}sg(G'_e)\dfrac{\gamma_e G'_e t^{(\pi/2)}_{1,\max}}{2L}, & sg(G'_e)\dfrac{t^{(\pi/2)}_{1,\max}}{L}\left(\dfrac{\gamma_e G'_e L}{2}+\Omega_1\right), & \dfrac{t^{(\pi/2)}_{1,\max}}{2\gamma_e G'_e L}\left(\Omega_1-\dfrac{\gamma_e G'_e L}{2}\right)^2 & \text{for a } \pi/2 \text{ pulse}\\ -sg(G'_e)\dfrac{\gamma_e G'_e t^{(\pi)}_{1,\max}}{L}, & -sg(G'_e)\dfrac{2\Omega_1 t^{(\pi)}_{1,\max}}{L}, & -\dfrac{\gamma_e G'_e L t^{(\pi)}_{1,\max}}{4} & \text{for a } \pi \text{ inversion pulse,}\end{cases} \tag{8b}$$

are coefficients depending on the overall durations $t^{(\pi/2)}_{1,\max}, t^{(\pi)}_{1,\max}$ over which any one of these rf pulses swept the $\gamma_e G'_e L$ frequency range spanned by the sample length L. Adding either one of these sweeps to the initial discrete excitation step leads

to a generic single-scan 2D encoding scheme of the kind illustrated in Fig. 4(A), whose overall phase evolutions prior to the mixing stage are

$$\varphi_{\text{encoded}} = \begin{cases} \varphi_{\text{exc}}(n,\delta z) + \varphi_{\text{sweep}}(z) & \text{for stored magnetizations } (\pi/2 \text{ chirp}) \\ -\varphi_{\text{exc}}(n,\delta z) + \varphi_{\text{sweep}}(z) & \text{for transverse magnetizations } (\pi \text{ chirp}). \end{cases} \tag{9}$$

Relying once again on Eq. (5b) to rewrite the z coordinate in terms of n and δz,

$$\begin{aligned} \varphi_{\text{encoded}}(n,\delta z) = {} & (\alpha q^2 \pm a)n^2 + (2\alpha qp + \beta q \pm b)n \\ & + (2\alpha q \pm c)n\delta z + (\beta + 2\alpha p \pm d)\delta z \\ & + \alpha(\delta z)^2 + \phi_{\text{rf}}(n) + \phi_{\delta z}, \end{aligned} \tag{10}$$

where the symbols are as defined in Eqs. (5), (7), and (8), and the $\pm$ accounts for the use of either storage or inversion chirped pulses.

As mentioned earlier, we decide to eliminate the undesired quadratic n dependence in Eq. (10) by setting

$$\phi_{\text{rf}}(n) = -(\alpha q^2 \pm a)n^2. \tag{11}$$

At the same time, the undesired differential slice dephasing proportional to $n\ \delta z$ is taken care of by setting the α parameter in the continuous sweep such that

$$\alpha = \mp c/2q. \tag{12}$$

Then, for a given set of chosen encoding parameters $(N_1, \Delta t_1, t_{1,\max}^{\text{chirp}})$, this condition fixes the ratio to be fulfilled by G_e/G_e'. All that remains in terms of the spin evolution's spatial encoding upon setting these parameters are then terms that depend on n and δz, according to

$$\varphi_{\text{encoded}}(n,\delta z) = \varphi_{\text{encoded}}(\delta z) + \xi n + C\frac{\Delta O}{\gamma_e G_e}\Omega_1 n, \tag{13a}$$

with

$$C = \begin{cases} \dfrac{t_{1,\max}^{(\pi/2)}}{L}\left(\dfrac{G_e'}{G_e} - 1\right) & \text{for the storage case} \\ \dfrac{2t_{1,\max}^{(\pi)}}{L}\left(1 - \dfrac{G_e'}{G_e}\right) & \text{for the inversion case,} \end{cases} \tag{13b}$$

a known constant under our control, and ξ another computable constant possessing no dependence on the internal couplings. As desired, the phase encoding in Eq. (13) is now linear in n and exhibits a pure δz intraslice dephasing terms defining the envelop of the signals.

In the full implementation of an ultrafast 2D experiment the indirect-domain spatial encoding just described is followed by a mixing process, and concluded by a postmixing gradient-driven acquisition. Such gradient succeeds, within a single transient, to correlate the indirect-domain Ω_1 evolution with the direct-domain Ω_2 interactions. To visualize how this gradient G_a—though constant throughout the data digitization—achieves this, we compute the additional acquisition phase that during this last stage of the experiment spins will accrue,

$$\begin{aligned} \varphi_{\text{acq}}(t_2) &= \gamma_a G_a z t_2 + \Omega_2 t_2 \\ &= \left[\gamma_a G_a\left(\frac{\Delta O}{\gamma_e G_e}(n - N_1/2) - \frac{\Omega_1}{\gamma_e G_e} + \delta z\right) + \Omega_2\right]t_2, \end{aligned} \tag{14}$$

where we have once again employed Eq. (5) to stress the stage's linear n dependence. This n dependence is in turn responsible for bringing all the excited elements in the discrete array represented by Eq. (13), back into phase and into an observable echo. (When dealing with a magnetization storage the ensuing amplitude modulation preserves two coherence pathways; as their nature is identical up to their sign we shall only handle one of them, arbitrarily chosen as the +1 pathway.) Disregarding from Eq. (14) the constant $N_1/2$-derived factor and recalling that in this constant-gradient acquisition case $k = \int_0^{t_2}\gamma_a G_a(t')dt' = \gamma_a G_a t_2$, the total phase expression then governing the direct-domain detection becomes

$$\begin{aligned} \varphi_{\text{total}}(n,\delta z,t_2) &= \varphi_{\text{encoded}}(n,\delta z) + \varphi_{\text{acq}}(t_2) \\ &= \xi n + C\frac{\Delta O}{\gamma_e G_e}\Omega_1 n + \frac{k}{\gamma_e G_e}\Delta O n \\ &\quad + \left(\Omega_2 - \Omega_1\frac{\gamma_a G_a}{\gamma_e G_e}\right)t_2 + \phi_{\text{dephase}}(k,\delta z). \end{aligned} \tag{15}$$

A constructive interference between the signals arising from different voxels will occur only when all the $n = 1,\ldots,N_1$ elements described by Eq. (15) are in phase. The mathematical equivalent for this condition is that the overall coefficient multiplying n is an integer multiple of 2π. This creates the desired linear relation between the location of an echo along the k axis and the indirect-domain Ω_1 interaction since, disregarding the ξn term acting as an overall offset that can be accounted for by the application of a preacquisition gradient pulse (see below), the position of the resulting echo peaks will then be

$$k = -C\Omega_1 + \frac{2\pi\gamma_e G_e}{\Delta O}m, \quad m = 0, \pm 1, \pm 2, \ldots\ . \tag{16}$$

As discussed in connection to Eq. (2) this expression implies that an unlimited number of k/ν_1 spectra will become available; in practice, enveloping effects determined by the $\phi_{\text{dephase}}(k,\delta z)$ term will place a limit to the number of spectral repetitions that appear. Assuming that T_p has been chosen long enough to obtain a sufficiently large number of echoes, one can use the spectral periodicity feature arising from Eq. (16) to derive a series of t_2-evolving indirect-

domain Ω_1 interferograms. The time gap between these adjacent indirect-domain spectra will be given by the periodicity interval $k_{\max}=2\pi\gamma_e G_e/\Delta O$ (Fig. 4), which when translated into Δt_2 increments equals $\gamma_e G_e/\Delta O\gamma_a G_a$. Given this constant dwell time between consecutive echoes one can then consider the rearrangement of a continuously digitized one-dimensional free induction decay $S(t)$ into a two-dimensional $S(k/\nu_1,t_2)$ matrix as presented in Fig. 4(B). Rescaling the indirect-domain axis and Fourier transforming the resulting data along t_2 one then obtains, according to the t_2 encoding in Eq. (15) and the k/ν_1 echoes defined by Eq. (16), 2D spectral line shapes appearing at frequencies

$$\left(\nu_1=-\frac{k}{C},\nu_2\right)=\left(\Omega_1,\Omega_2-\Omega_1\frac{\gamma_a G_a}{\gamma_e G_e}\right). \tag{17}$$

Besides the joint Ω_1/Ω_2 influences that this expression predicts along the direct domain, and which can be accounted for by a simple shearing of the data, the desired 2D spectrum is thus exactly as desired. Its bandwidth and resolution characteristics are similar to those defining other ultrafast 2D NMR acquisitions;[21] but this one was obtained by setting only three different gradient values (G_e, G_e', and G_a) left constant through relatively long evolution and acquisition times. The multiple gradient oscillations that were previously needed to jointly sample the two spectral domains are thus eliminated.

III. EXPERIMENTAL RESULTS

Tests on the performance of the protocol just described (as well as of its sensitivity-enhanced variant introduced in the coming section) were carried out on a Varian iNova® NMR spectrometer and HCN probe operating at a 501 MHz Larmor frequency. As this new protocol—just as its conventional 2D time-domain counterpart—is governed by a variety of parameters controlling resolution and bandwidth along both spectral domains, a variety of choices had to be made. Particularly important among these were the number N_1 of discrete elements to be excited; we found that, in general, setting $N_1=24$ provided spectra of sufficient quality for typical homonuclear acquisitions. The resulting trains of N_1 overlapping excitation rf pulses required by this methodology were created according to the principles described in the preceding section, leading to a single, continuous rf excitation module built by adding up a series of time- and frequency-shifted $\pi/2$ excitation wave forms. Each of the coadded excitation pulses was given a WURST-type amplitude-modulated shape, and potential Bloch-Siegert interferences among the constituent wave forms were neglected in view of the good performance of the experiments. These considerations were used to generate a single amplitude- and phase-modulating rf table, which was read out at an appropriate clocking rate by the spectrometer's waveform generators. The waveforms of the subsequent storage/inversion chirped rf pulses were calculated using similar principles according to the guidelines given in the previous section. The calculation of all the resulting rf shapes, as well as all the postexperimental data processing required by the experiments, were implemented using custom-written MATLAB® software packages.

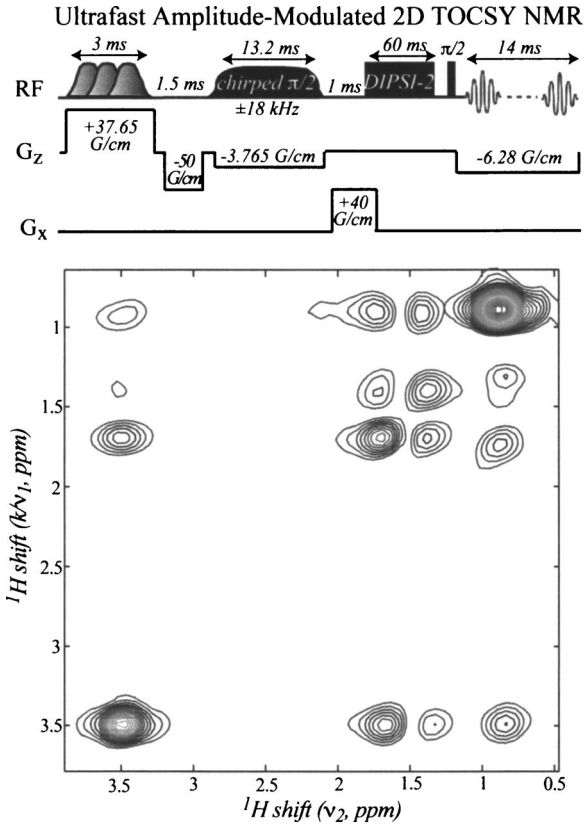

FIG. 5. Ultrafast 2D TOCSY NMR spectrum of *n*-butylchloride/DMSO-d_6 recorded utilizing the pulse sequence indicated on top and the indicated timing, gradient amplitude, and frequency-chirping parameters. Additional experimental settings included $N_1=24$, $T_p=2$ ms, $\Delta t_1=0.045$ ms, $\Delta O=12$ kHz, a 2 μs physical acquisition dwell time, and $\approx$50 kHz analog filtering of the data. Two scans differing in the phases of the excitation pulse train and of the receiver were coadded in order to better eliminate the contributions arising from the unencoded sample. Signal processing involved arranging the collected FID into a 50×28 $(k/\nu_1,t_2)$ data matrix, zero filling to 128×64, smoothing of sharp enveloping effects along both dimensions by weighting with QSIN filters, 1D FT of the data along t_2, shearing according to Eq. (17) to obtain a conventional-looking TOCSY spectrum, and plotting of the data in magnitude mode.

A first example of the new concepts here introduced is illustrated in Fig. 5, which presents an ultrafast 2D TOCSY NMR spectrum collected on a *n*-butylchloride/DMSO-d_6 sample. This experiment involved the application of three basic gradient periods as described above: a constant G_e value for effecting the discrete excitation, a continuous $\pi/2$-based swept storage of the indirect-domain magnetization during the course of a G_e' gradient, and a final G_a gradient kept constant throughout the course of the data acquisition. In addition to these three essential elements, two auxiliary gradients were used: the first one, positioned immediately after the initial pulse train, was applied in order to account for the ξn offsetlike term introduced in Eq. (13) and thereby center the indirect-domain spectrum at a convenient position along the final k/ν_1 axis. A second gradient pulse was applied along an orthogonal axis following the storage of the spatially encoded information to better suppress any residual non-longitudinal magnetization: as most spins in the sample have been excited by the second, continuous chirped pulse rather than by the initial sparse discrete excitation, this

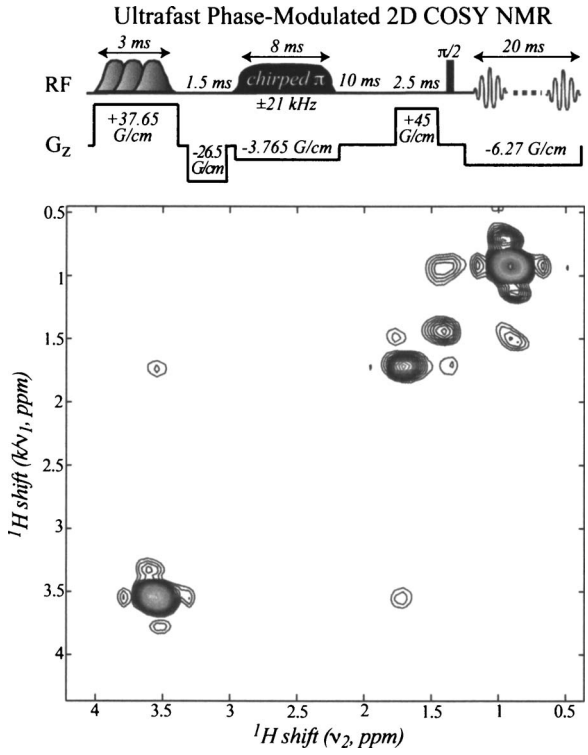

FIG. 6. Ultrafast H,H-COSY NMR spectrum of n-butylchloride/DMSO-d_6, illustrating the potential of the new constant-gradient acquisition protocol to record phase-modulated 2D data. The encoding, acquisition, and processing parameters used in this experiment were nearly identical as in Fig. 5; main differences entailed the nature of the mixing process, with a free evolution delay and a hard $\pi/2$ pulse replacing the previous isotropic mixing, and the chirped refocusing stage, with a π chirped pulse capable of preserving all coherences within the x-y plane replacing the $\pi/2$-driven storage of magnetizations previously used.

auxiliary gradient (as well as phase cycling) helps purge the spectrum of undesired coherences. Although these ancillary gradients are not essential their execution does not exceed the demands normally associated with gradient-enhanced NMR spectroscopy; hence their addition was deemed reasonable. Further details on this amplitude-modulated experiment, whose spectrum shows all the features expected from a conventional 2D TOCSY correlation, are given in the corresponding figure and caption.

The new ultrafast 2D acquisition scheme described in the preceding section can also be used for the execution of phase-modulated sequences, by replacing the $\pi/2$ storage chirped pulse employed in Fig. 5 by an in-plane π sweep. The resulting encoding pattern can then be exploited for certain sequences that do not support amplitude modulation over the indirect domain, for instance, the homonuclear 2D COSY NMR experiment. Figure 6 illustrates an example of such discrete-$\pi/2$ / continuous-π procedure, which leaves transverse in- and antiphase coherences in the x-y plane following the indirect-domain encoding. Following a short ($\approx 1/4J$) delay for enhancing the coherence transfer, a hard $\pi/2$ pulse could then be applied to impart the desired intersite mixing cross peaks via an $I_z S_\alpha \rightarrow I_\alpha S_z$ transfer. Subjecting the n-butylchloride/d_6-DMSO model sample to this pulse sequence clearly provides all the expected nearest-neighbor cross peaks. Considerations similar to those detailed for the TOCSY sequence also make this case susceptible to additional spectral improvements, via the application of short pair of auxiliary gradient pulses. Once again, all the observed spectral features are as expected from a conventional 2D acquisition.

A special case worth remarking in connection with the use of π chirp pulses and of the ensuing phase modulation arises in the particular case when G_e is chosen identical to G'_e. The spatiotemporal coefficient C in Eq. (13) becomes then zero, and as a consequence one appears to obtain a complete elimination of the indirect-domain interactions. This conclusion, however, is in this case deceptive. On one hand, as homonuclear J couplings will remain effectively invariant to π rotations of both intervening species, the spatial encoding effects imparted by this evolution will persist. It can be shown that homonuclear J couplings will still be imparted over the indirect-domain evolution, with a spatiotemporal coefficient $C_J = -2t^{(\pi)}_{1,\max}/L$. As for chemical shift effects, although their net indirect-domain encoding will be effectively zero they will have an effect on the actual positions of the z_n voxels excited, and hence will appear involved in the shearing defining peak positions along ν_2. The fact that differing coefficients scale the indirect-domain effects of the shift and coupling interactions calls for a redefinition of the spectral positions introduced in Eq. (17), derived under the assumption that the Ω_1 interactions that defined the z_n voxels excited were the same as those defining the indirect-domain encoding. Now, however—and in other conceivable instances involving heteronuclear decoupling/recoupling periods during portions of t_1—the Ω_1 defining the positions of the excited slices will involve both J couplings and chemical shifts, whereas the Ω_1^{eff} defining echoes along k/ν_1 will only reflect the J couplings. Moreover, taking into account the reversal that the chemical shift Hamiltonian H_{cs} (but not its homonuclear J-coupling counterpart H_j) effectively undergoes upon being subject to a π inversion, we can redefine the positions of peaks in the 2D spectrum as

$$\left(\nu_1 = -\frac{k}{C_{\text{eff}}}, \nu_2\right) = \left(\Omega_1^{\text{eff}}, \Omega_2 + \Omega_1 \frac{\gamma_a G_a}{\gamma_e G_e}\right), \tag{18}$$

where Ω_1^{eff}, Ω_1, and Ω_2 are Bohr frequencies defined by the H_J, $-H_{\text{cs}}+H_J$, and $H_{\text{cs}}+H_J$ interactions, respectively. With these provisions in mind the resulting J-derived winding pattern will, just as in the more conventional instances exemplified above, be susceptible to unraveling by a constant acquisition gradient. As both chemical-shift and homonuclear J-coupling interactions are involved in the definition of the Ω_1 and Ω_2 frequencies, this means that the correlation will provide some kind of J-resolved 2D homonuclear spectrum.[1,26] Interestingly, the built-in experimental shearing factor in Eq. (18) means that the net shifts and couplings observed along the direct ν_2 domain can in principle be controlled by changing the size and sign of the gradient G_a unraveling the effective J encoding imposed during the action of $G_e = G'_e$. This leads to the possibility of achieving a net increase or net canceling of either the shifts or the couplings detected along the ν_2 axis by means of gradients, rather than by executing numerical postacquisition treatments of the acquired data. Such unusual behavior was tested on a solution

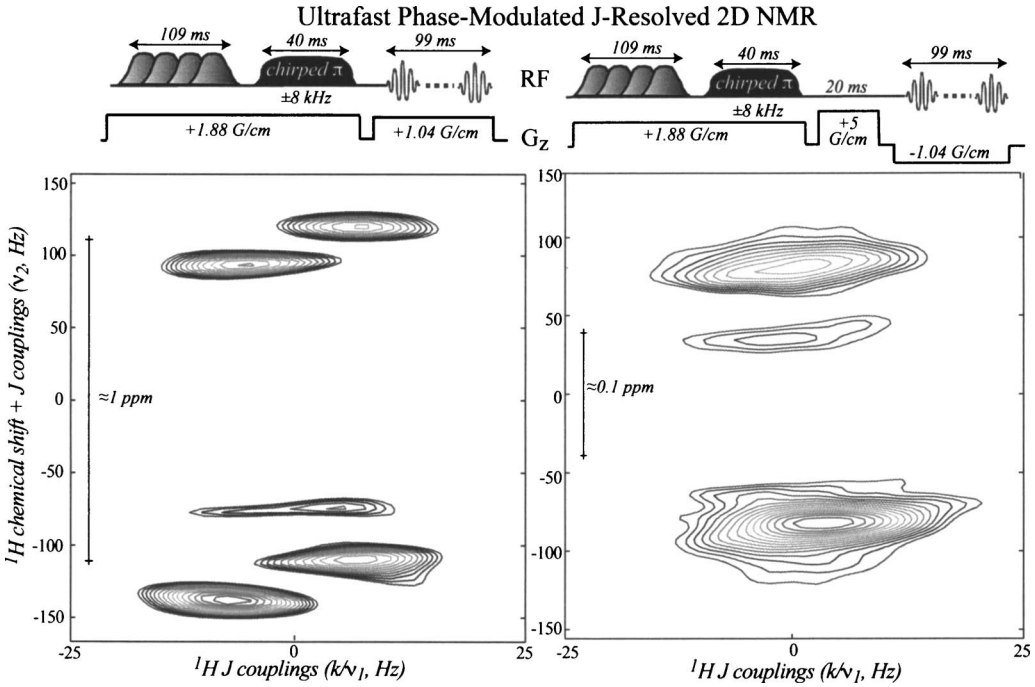

FIG. 7. Different implementations of the 2D *J*-resolved ultrafast NMR constant-gradient experiment on a cinnamic acid/DMSO-d_6 solution. Both acquisitions were carried out with the indicated parameters and $N_1=24$, $T_p=40$ ms, $\Delta t_1=3$ ms, and $\Delta O=0.6$ kHz, using $G_e=G'_e$ plus a chirped rf π sweep for the sake of encoding only the homonuclear couplings along the indirect domain. Following a suitable data processing procedure, the displayed spectra were observed. Different patterns arise in the left- and right-hand panels owing to the opposing signs used for the acquisition gradients decoding the *J* pattern; this, in spite of the symmetric frequency encoding arising from the effects of the spin-spin *J* coupling. As further explained in the text the application of equally signed G_e's and G_a's increases the effective *J* coupling and reduces the effective chemical shift, while unequally signed gradients influence the spectrum in the opposite manner. This leads to different scaling factors of the shift-related ppm values along direct-domain frequency axis (arrows): 225 in the left-hand panel, and 777 Hz/ppm in the right-hand one. Notice that as the direct domain spectral ranges that were measured corresponded to 330 Hz in both cases, spectral folding occurred along the ν_2 axis of the latter panel.

of cinnamic acid dissolved in DMSO-d_6, which targeted along the indirect domain the $\approx$16 Hz homonuclear *J*-coupling active between the olefinic protons. On choosing the appropriate signs for the encoding and acquisition gradients the effective direct-domain splittings become scaled by a factor of $(1+|G_a/G_e|)$, leading as shown in Fig. 7(A) to an experimental value of 25 Hz. By contrast choosing the same strengths but opposite signs for this pair of gradients leads to a nearly null $(1-|G_a/G_e|)$ *J*-scaling factor, and thereby to a spectrum evidencing homonuclear *J* decoupling along its direct frequency domain [Fig. 7(B)]. Notice as well the concurrent and opposing scaling of the chemical shift effects affecting these differing choices of gradient signs along the direct-domain frequency axis; all of this as predicted by the arguments surrounding Eq. (18).

IV. SENSITIVITY-ENHANCED CONSTANT-GRADIENT ULTRAFAST 2D NMR

The basic requirement of the new experiments hitherto described is that the discrete individual elements employed in the encoding be made sufficiently narrow *vis-á-vis* their spatial separation. Indeed as mentioned in connection to Eq. (4), only if the pulse lengths T_p are made sufficiently long in comparison with the interpulse offset incrementation ΔO will a reasonable number of N_2 interferograms become available for reconstructing the direct-domain spectral frequencies. For the fixed-frequency, amplitude-modulated $P(t)$ rf pulse shapes assumed in the preceding section, this in turn implies that only a small fraction of the sample will actually be used in the experiment. This fraction is in the order of the bandwidth excited by each of the pulses divided by the frequency incrementation between pulses: $(T_p)^{-1}/\Delta O \sim 1/N_2$. For conventional N_2 choices attempting to accommodate multiple echoes within a single scan this fraction will evidently be small, leading to an ensuing loss in sensitivity that will compound the intrinsic penalties associated with conventional ultrafast 2D NMR.[21] Analogous losses are known to affect single-scan BURST imaging techniques of the kind illustrated in Fig. 3(B). For this family of techniques, however, it has been shown that sensitivity could be partially recouped by modulating the fixed-frequency pulses involved in the DANTE excitation train by a frequency-modulated (FM) envelope.[27] Such route cannot be copied for enhancing the sensitivity of the constant-gradient 2D NMR acquisition mode discussed in this work, given the different operational principles of the imaging and spectroscopic experiments. Still, a FM-based ultrafast 2D NMR variation can be devised, which provides an analogous sensitivity gain; such is the topic of the present section.

A summary of the changes that we propose to enhance the sensitivity of our original pulse sequence based on the use of FM rf pulses is illustrated in Fig. 8. Notice that in this case the central offsets, timings, phases, nutation angles, and gradient considerations involved in the overall design of the encoding processes remain identical to the various counterparts that were presented earlier. A main difference, however,

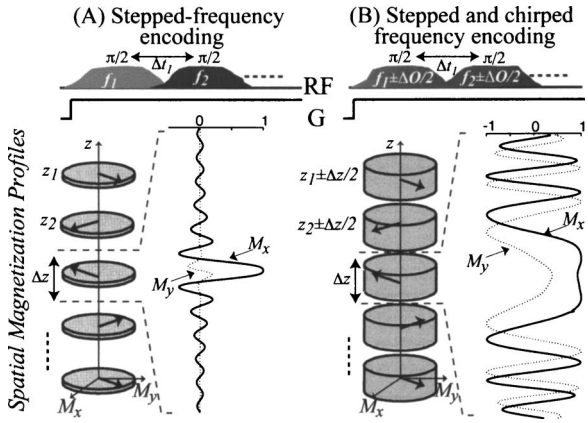

FIG. 8. Enhancing the sensitivity of the constant-gradient ultrafast acquisition protocol by imposing an additional frequency modulation on its train of discrete encoding pulses. In the original scheme (A) pulses were chosen at fixed frequencies $\{f_i\}_{i=1,N_1}$ with equal steps $\Delta O=|f_{i+1}-f_i|$ and long pulse durations T_p yielding narrow, well-separated excitation voxels. As a result of these settings only a small fraction of the available spin magnetization, on the order of $1/N_2$, is employed within each spatial step $\Delta z=\Delta O/\gamma_e G_e$. By contrast, sweeping the frequency f of each of the encoding pulses between $-\Delta O/2+f_i \leqslant f \leqslant \Delta O/2+f_i$ values broadens the excitation profile associated with each offset (B), leading to an increase in the amount of spins contributing to the experiment's final signal.

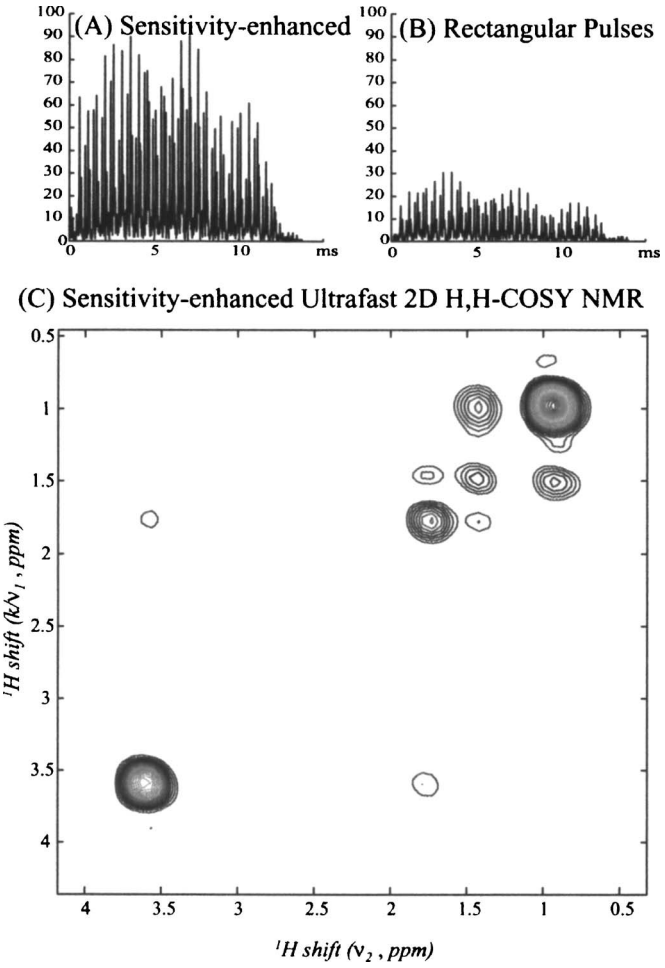

FIG. 9. Comparison between the performances observed upon utilizing a FM *vis-à-vis* a constant-amplitude $P(t)$ rf pulse shape for the execution of a discrete ultrafast NMR excitation. (A) As-collected FID (magnitude) obtained by a pulse sequence identical to that leading to the H,H-COSY spectrum presented in Fig. 6, except for the fact that the original train of WURST-shaped frequency-stepped pulses has been replaced by a series of frequency-stepped chirped pulses. Setting the sweeping range of these selective rf pulses equal to the ΔO frequency increment (12 kHz) leads to a larger proportion of the sample being excited. Compared to the FID acquired by the scheme of Fig. 6(B), the signal has improved by a factor ≈ 3. Following the additional quadratic phase correction and processing as described in the text, appearance of the sensitivity-enhanced ultrafast H,H-COSY spectrum (C) is still as expected.

now arises from the fact that in order to enhance the sensitivity, the offsets of the individual rf pulses are modulated so as to sweep the entire range of frequencies ΔO—including the regions that had previously remained unexcited. Thus replacing the fixed frequency pulses used so far by a train of chirped rf pulses, still of overall duration T_p but now exciting spins over a $\pm\Delta O/2$ range about their $\{f_n\}_{n=1,N_1}$ central frequencies, can be used to achieve a full excitation of spins throughout the sample. A straightforward way of visualizing how the reliance on such FM chirped procedures will affect the overall scheme of the ultrafast 2D NMR acquisition consists of assuming that all experimental parameters and definitions pertaining to the experiment remain the same, apart for an alteration of the $P(t)$ envelopes that used to define all rf pulse shapes. Whereas such pulse shapes were hitherto assumed to entail a simple rectangular (or in the actual experimental examples given in Figs. 5–7, a WURST-type) amplitude modulation, it is possible to account for the additional FM that is now being imposed by assuming that every $P(t)$ pulse shape has become a complex function encompassing an offset sweep $O(t)=\Delta O(t/T_p-1/2)$. This sweep will transform an ideal rectangular rf pulse shape into

$$P(t)=\begin{cases}\exp\left(-2\pi i\int_0^t O(t')dt'\right), & 0<t<T_p\\ 0, & o.w.\end{cases}.$$

The quadratic temporal dependence characterizing the phase of this pulse will in turn be imprinted into the $E(k)$ enveloping function as described in Eq. (3), thereby affecting the phases displayed by the N_2 indirect-domain echoes along the data acquisition. The convenience of casting the experiment in this fashion stems from the fact that it allows us to maintain all the definitions and conditions derived earlier for the various stages of the ultrafast NMR experiment unchanged, and account for all the consequences of adding a FM onto the rf pulses by an additional phase modulation of the echoes to be detected. Like was the case for its rf $P(t)$ counterpart, this additional phase modulation of the signals observed along t_2 will have a quadratic time dependence that operates on top of the Ω_2 modulation, and that could therefore mask the direct-domain frequencies being sought. This additional quadratic modulation, however, is entirely known—reflecting under the linear approximation being used throughout this analysis, the phase imposed onto the $P(t)$ in a one-to-one fashion. Its effect can therefore be removed entirely by a suitable numerical phase correction of the collected $S(k/\nu_1,t_2)$ interferogram, prior to subjecting the resulting data to 1D FT along t_2.

To test the feasibility and sensitivity-enhancing characteristics of the resulting frequency-swept encoding modality,

an additional series of ultrafast H,H-COSY experiments was recorded. Figure 9 shows a phase-modulated constant-gradient 2D spectrum acquired under parameters identical to those shown in Fig. 6; the only difference between this previous experiment and the current one being the replacement of the fixed-frequency WURST-type rf pulses in charge of the spatial encoding by smoothed chirped pulses, sweeping over the same $T_p=2$ ms pulse times the full $\Delta O=12$ kHz band gap defining the separation among the various $\{f_n\}_{n=1,N_1}$ offsets. As can be appreciated the overall spectral features resulting from the chirped-based acquisition are, following the quadratic temporal correction of the echoes and subsequent 1D FT, entirely as expected for this compound. Moreover, a comparison between the absolute signal intensities retrieved using this alternative chirped approach shows a considerable enhancement *vis-à-vis* the one obtained with the previous constant-frequency method. This is illustrated in Figs. 9(A) and 9(B), which evidence an approximately threefold increase in the signal's amplitude using the modified procedure.

Although the observed enhancement is significant, it also reveals that the proportion of the sample contributing to the experimental signal is still far from unity. Indeed, given the $N_1=24$ excitation pulses being used, it follows that the conventional square-shaped protocol employed only $100/24 \approx 4.1\%$ of spins in the sample; when multiplied by the experimentally detected enhancement factor still denotes a use of slightly more than 12% of all spins present. The fact that in spite of having been excited in their entirety not all spins contribute to the observable 2D spectrum parallels a similar effect arising when imposing a FM envelope modulation on the single-scan DANTE-based imaging sequence.[27] In the present ultrafast spectroscopy case this can be understood by comparing the changes affecting the spatial profiles that are excited upon altering the original constant-amplitude squarelike pulses used in the preceding section, into the chirped FM pulses introduced now for achieving the sensitivity enhancement. These profiles (M_x and M_y traces in Fig. 8) illustrate how upon going from a constant amplitude to a FM rf pulse shape there is indeed a significant increase in the region over which spins are excited; they also denote the onset of a strong quadratic phase modulation within each of these extended spatial profiles. This rapid phase modulation, affecting at any one time different positions within the excited spatial voxels, results in a destructive interference among the signals arising from spins in these regions that prevents the full realization of a maximum enhancement. The effective enhancement arises solely from the widened region displaying the slower phase modulation, which for the case of simple chirped pulses such as the ones under considerations can be approximated as $\Delta z_{\mathrm{chirp}} \approx (1/\gamma_e G_e)\sqrt{2\pi\Delta O/T_p}$.[28] When compared with the spatial extent excited by a nonmodulated squarelike pulse, $\Delta z_{\mathrm{square}} \approx 2\pi/\gamma_e G_e T_p$ this predicts that sensitivity will be enhanced by a factor $\Delta z_{\mathrm{chirp}}/\Delta z_{\mathrm{square}} \approx \sqrt{\Delta O T_p/2\pi}$; or [*qv*. Eq. (4)] by a factor $\sqrt{N_2}$. For the $N_2=24$ value used in Fig. 9 this prediction is in fairly good agreement with the experimentally observed enhancement factor.

V. CONCLUSIONS

The present work introduced a new strategy for the acquisition of ultrafast 2D NMR data, which adds to a growing family of protocols available for the execution of this kind of experiments. By contrast to the variants that have hitherto been discussed the one that has been here derived and exemplified differs by being free from the need to repetitively switch the ancillary field gradients involved in the 2D experiment—both during the spatial encoding, as well as during the course of the gradient-driven data acquisition. In this regard its execution is considerably simpler than the alternatives that had been discussed, all of which required the use of rapidly alternating periodic gradients during the course of the data acquisition. We believe that this newly found independence from the need to rapidly oscillate the acquisition gradients could be valuable when executing this kind of experiments on a variety of systems, particularly those for which the duration taken by multiple gradient switching oscillations proofs unacceptably long. Examples of these can be expected upon attempting to implement ultrafast 2D acquisitions on certain large-bore or unshielded spectroscopic MRI scanners, as well as when attempting the implementation of these experiments in wideline solid state NMR and/or electron paramagnetic resonance scenarios involving rapidly relaxing spins. The need for removing the multiple gradient oscillations might also prove advantageous for facilitating the ultrafast acquisition of higher-dimensional experiments.

In order to lift the need to oscillate the gradients over the course of the acquisition, the present study relied on a new ultrafast 2D encoding approach based on what had hitherto been considered mostly an artifact: the "ghosting" effects arising upon using a discrete spatial excitation. These phenomena, and their underlying mathematical principle stating that spectra can be decoded multiple periodical times if originating from a discrete, equidistant set of spin isochromats, make it possible to decode the complete information of a spatially encoded 2D NMR spectrum even if relying on a constant gradient. Still, this mode of operation is not without its penalties or limitations. Foremost among its drawbacks is the need to operate with narrowband excitation slices to enable the generation of long-lived, multiple-echoed interferograms, a feature that compromises the limited sensitivity usually available in ultrafast 2D NMR acquisitions. It was for the sake of alleviating this feature that a sensitivity-enhanced variant of the experiment was derived and demonstrated, and even though only a partial compensation of the sensitivity lost by the discrete narrowbanded encoding could be achieved by this discrete FM-based procedure, it is likely that more sophisticated versions of the simple linear frequency sweep here assayed can successfully attain higher degrees of enhancement. Another potential drawback of the new strategy that was here introduced concerns the effects that molecular diffusion could have in the sensitivity of the experiment. Although the comparative effects of diffusion on the different ultrafast encoding sequences have not yet been considered in detail, it is reasonable to expect that acquisition sequences such as the ones that have been hereby

discussed—relying heavily on nearly constant gradients—will exhibit stronger motion-related attenuation effects than their fast-oscillating counterparts. This is a feature that could be viewed as a drawback, but also exploited within a context of monitoring motions in combination with spectroscopic resolution. All of these options are at the moment targets of further analysis and experiments.

ACKNOWLEDGMENTS

This work was supported by the Israel Science Foundation (ISF 1206/05), the German-Israel Fund (GIF 782/2003), the US-Israel Binational Science Foundation (BSF 2004298), and the U.S. National Institutes of Health (GM-72565).

[1] R. R. Ernst, G. Bodenhausen, and A. Wokaun, *Principles of Nuclear Magnetic Resonance in One and Two Dimensions* (Clarendon, Oxford, 1987).
[2] J. Cavanagh, W. J. Fairbrother, A. G. Palmer, and N. J. Skelton, *Protein NMR Spectroscopy: Principles and Practice* (Academic, San Diego, CA, 1996).
[3] *Encyclopedia of NMR*, edited by D. M. Grant and R. K. Harris (Wiley, Chichester, 1996).
[4] J. Jeener, *Ampere International Summer School II* (Basko Polje, Yugoslavia, 1971).
[5] W. P. Aue, E. Bartholdi, and R. R. Ernst, J. Chem. Phys. **64**, 2229 (1976).
[6] L. Frydman, T. Scherf, and A. Lupulescu, Proc. Natl. Acad. Sci. U.S.A. **99**, 15858 (2002).
[7] L. Frydman, T. Scherf, and A. Lupulescu, J. Am. Chem. Soc. **125**, 9204 (2003).
[8] Y. Shrot and L. Frydman, J. Am. Chem. Soc. **125**, 11385 (2003).
[9] N. Sela, H. Degani, and L. Frydman, Magn. Reson. Med. **52**, 893 (2004).
[10] B. Shapira, A. Karton, D. Aronzon, and L. Frydman, J. Am. Chem. Soc. **126**, 1262 (2004).
[11] B. Shapira, E. Morris, A. K. Muszkat, and L. Frydman, J. Am. Chem. Soc. **126**, 11756 (2004).
[12] M. Gal, M. Mishkovsky, and L. Frydman, J. Am. Chem. Soc. **128**, 951 (2006).
[13] P. Pelupessy, J. Am. Chem. Soc. **125**, 12345 (2003).
[14] Y. Shrot, B. Shapira, and L. Frydman, J. Magn. Reson. **171**, 162 (2004).
[15] A. Tal, B. Shapira, and L. Frydman, J. Magn. Reson. **176**, 107 (2005).
[16] N. S. Andersen and W. Köckenberger, Magn. Reson. Chem. **43**, 795 (2005).
[17] B. Shapira, Y. Shrot, and L. Frydman, J. Magn. Reson. **178**, 33 (2006).
[18] Y. Shrot and L. Frydman, J. Magn. Reson. **164**, 351 (2003).
[19] M. S. Cohen, R. M. Weisskoff, R. R. Rzedzian, and H. L. Kantor, Magn. Reson. Med. **14**, 409 (1990).
[20] P. Mansfield and P. R. Harvey, Magn. Reson. Med. **29**, 746 (1993).
[21] B. Shapira, A. Lupulescu, Y. Shrot, and L. Frydman, J. Magn. Reson. **166**, 152 (2004).
[22] J. Hennig and M. Hodapp, MAGMA (N.Y.) **1**, 39 (1993).
[23] I. J. Lowe and R. E. Wysong, J. Magn. Reson., Ser. B **101**, 106 (1993).
[24] L. Zha and I. J. Lowe, Magn. Reson. Med. **33**, 377 (1995).
[25] G. A. Morris and R. Freeman, J. Magn. Reson. **29**, 433 (1978).
[26] W. P. Aue, J. Karhan, and R. R. Ernst, J. Chem. Phys. **64**, 4226 (1976).
[27] Z. H. Cho, Y. M. Ro, and I. K. Hong, Concepts Magn. Reson. **10**, 33 (1998).
[28] Y. Shrot and L. Frydman, J. Magn. Reson. **172**, 179 (2005).